Hindawi Publishing Corporation
Advances in Optical Technologies
Volume 2012, Article ID 676785, 6 pages
doi:10.1155/2012/676785

Research Article

Continuous Operation of a Bragg Diffraction Type Electrooptic Frequency Shifter at 16 GHz with 65% Efficiency

Shintaro Hisatake, Kenji Hattori, and Tadao Nagatsuma

Graduate School of Engineering Science, Osaka University, Toyonaka, Osaka 560-8531, Japan

Correspondence should be addressed to Shintaro Hisatake, hisatake@ee.es.osaka-u.ac.jp

Received 15 July 2012; Accepted 22 September 2012

Academic Editor: Borja Vidal

We demonstrate for the first time the continuous operation of a Bragg diffraction type electrooptic (EO) frequency shifter using a 16 GHz modulation signal. Because frequency shifting is based on the Bragg diffraction from an EO traveling phase grating (ETPG), this device can operate even in the millimeter-wave (>30 GHz) range or higher frequency range. The ETPG is generated based on the interaction between a modulation microwave guided by a microstrip line and a copropagating lightwave guided by a planner waveguide in a domain-engineered $LiTaO_3$ EO crystal. In this work, the modulation power efficiency was improved by a factor of 11 compared with that of bulk devices by thinning the substrate so that the modulation electric field in the optical waveguide was enhanced. A shifting efficiency of 65% was achieved at the modulation power of 3 W.

1. Introduction

Coherent optical frequency conversion based on external modulation is an important technique not only for the optical communication and optical measurement but also for microwave and millimeter-wave photonics because it corresponds to an upconversion from RF to optical domain. Photomixing of two optical modulation sidebands generated by an electrooptic phase modulator (EOM) or a frequency comb generator has been used to generate low phase noise coherent microwaves or millimeter-waves, which are desirable for many applications such as the radar [1], sensing [2–4], and wireless communications [5]. The advantages of the external modulation method over other methods such as optical injection locking, optical phase-locked loop, and dual-wavelength laser source are the system's simplicity, stability, and frequency tunability. However, typical sinusoidal phase modulation is an inherently inefficient method of frequency conversion. At best, the fraction of the power in the first-order sideband generated by normal phase modulation is theoretically $(J_1(\beta))^2 \approx 34\%$, where $J_1()$ is a first-order Bessel function of the first kind and β is the modulation depth. The conversion efficiency of 34% corresponds toan extra loss of about 5 dB. Because the noise figure (NF) of an optical amplifier is relatively poor compared to electronic amplifiers, extra loss due to a low conversion efficiency impacts most key aspects of microwave and millimeter-wave photonics in which low-loss 1550 nm components should be used [6, 7]. The lower conversion efficiency results in a lower carrier-to-noise ratio (CNR). The higher conversion efficiency is essential not only for microwave and millimeter-wave photonics applications but also for other photonic applications in which the system performance is governed by the CNR.

Recently, we proposed a new-type of EO frequency shifter and experimentally demonstrated the 16.25 GHz frequency shift with 82% efficiency [8]. The operation is based on the Bragg diffraction from an EO traveling phase grating (ETPG). Because the ETPG is produced based on the Pockels effect, this shifter can operate in the millimeter-wave (>30 GHz) range or in the higher frequency range. Moreover, multiplication of the frequency shift can be realized by cascading the ETPGs. We demonstrated a frequency shifting of ±32.5 GHz with a 60% efficiency, using a 16.25 GHz modulation signal (doubler operation) [9]. Together with recent progressive high-speed modulation technologies [10],

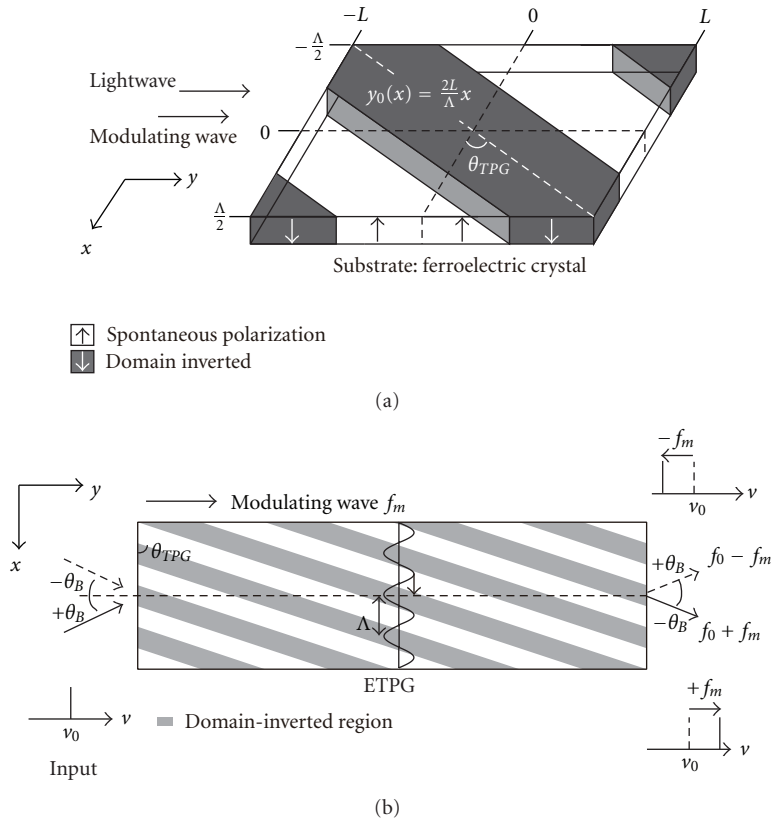

Figure 1: (a) Basic structure of the domain-inverted ferroelectric crystal. The width and the center position of the domain-inverted region are L and y_0, respectively. (b) Schematic of the frequency shifting operation.

multiplication of the Bragg diffraction from the ETPG promises to realize the terahertz (>100 GHz) coherent link with high efficiency (more than Bessel function). However, bulk devices previously reported required relatively higher modulation power, typically several tens of watts at 16 GHz, therefore they were driven with pulsed magnetron.

In this paper, we demonstrate a waveguide-based frequency shifter in which the modulation power is significantly reduced compared with bulk shifters. A planar waveguide is fabricated using a conventional proton exchange method in a congruent $LiTaO_3$ (CLT) EO crystal [11]. The modulation electrode is a microstrip line. To improve the modulation efficiency, we reduced the thickness of the substrate, that is, the distance between the hot and ground electrodes, from 0.5 mm in the former bulk device to 0.1 mm.

In Section 2, the principle of the ETPG and frequency shifting are briefly summarized. Section 3 discusses the improvement of the modulation power efficiency by reducing the thickness of the substrate. In Section 4, we summarize the design and fabrication of the waveguide-based frequency shifter. Experimental results and discussions are summarized in Section 5.

2. Principle of the Frequency Shift Based on the ETPG

We briefly explain the principle of the frequency shift based on the ETPG. The ETPG is a time-varying phase distribution within the optical beam cross-section produced by an interaction between the traveling modulation wave and the copropagating lightwave in a periodically domain-inverted (polarization-reversed) EO crystal. Figure 1(a) shows the basic structure of the domain-inverted EO crystal. The device is formed by repeating this basic structure and arranging the repeated structure in two dimensions on the x-y plane. When a lightwave with the group velocity of v_o propagates along the y-axis with a collinear traveling modulation wave with the phase velocity of v_m in the crystal, the modulating electric field $E(y, t_0)$, which the lightwave entering the device at time t_0 encounters at position y, can be written as $E(y, t_0) = E_m \cos(2\pi f_m t_0 - \pi y/L)$, where E_m is the amplitude of the modulating wave, f_m is the modulation frequency, and $L = 1/(2f_m(1/v_m - 1/v_o))$. From this equation, we find that the traveling phase grating can be realized by setting the length and the center position of the domain-inverted region to be L and $y_0(x) = 2Lx/\Lambda$, respectively. The phase shift induced to a light passing through the length of $2L$ of this domain-inverted crystal, which is shown in Figure 1(a), is expressed as

$$\begin{aligned}\Delta\phi(x,t) &= \Delta\phi_m \sin\left(2\pi f_m t_0 + \frac{\pi y_0(x)}{L}\right) \\ &= \Delta\phi_m \sin(2\pi f_m t_0 + \beta x),\end{aligned} \tag{1}$$

where $\Delta\phi_m$ is the modulation index and $\beta = 2\pi/\Lambda$. This resultant phase distribution expresses a traveling sinusoidal

phase grating pumped by the electrical modulation signal. We refer to this time-varying phase distribution as the ETPG. Operation of the acoustooptic (AO) frequency shifter is based on the Bragg diffraction from the traveling phase grating pumped by an acoustic wave. Based on the analogy with the AO frequency shifter, we can realize the EO frequency shifter based on the Bragg diffraction from the ETPG [8].

The remarkable features of the ETPG are (1) the period of the ETPG is determined by the period (Λ) of the domain inversion in the x direction, not by the wavelength of the modulating wave, and (2) the traveling direction of the ETPG is determined by the sign of the β, that is, the sign of the tilting angle (θ_{TPG}) of the periodic domain inversion. The first feature allows the ETPG to operate at a higher modulation frequency even at the millimeter-wave frequency. The second feature allows us to cascade the ETPG to accumulate frequency shifting (multiplication) [9].

3. Improvement of the Modulation Power Efficiency

Although the proton exchange process might degrade the Pockels effect [12], in this section, we will confirm experimentally the effect of reducing the thickness of the substrate on the improvement of the modulation efficiency. We fabricated waveguide devices with four different thicknesses t and measured the modulation efficiency, which is defined as the modulation index per interaction length per modulation power (rad/mm/W). Figures 2(a) and 2(b) show a cross-section view of the conventional bulk device and the proposed waveguide device, respectively. The substrate is a congruent $LiTaO_3$ (CLT) EO crystal. The lightwave and modulation microwave propagate along the y direction. The traveling modulation microwave is guided by the microstrip line. The SiO_2 buffer layer is deposited on the waveguide before evaporating the hot electrode of the microstrip line to reduce propagation losses. The thickness of the buffer layer is about 0.1 μm. The depth of the waveguide is about 0.8 μm for single mode operation, which will be discussed later.

Figure 3 plots the modulation efficiency of the waveguide device for $t = 0.1$, 0.15, 0.3, and 0.5 mm. The modulation efficiencies are normalized by the values obtained with the 0.5-mm bulk device. The dashed line is the theoretical function ($\propto 1/t^2$) fitted to the data. Because of the proton exchange process, the experimentally achieved modulation efficiency of the waveguide device was reduced to about 50% of that of the bulk device. The modulation efficiency improved inversely proportional to the square of the device thickness, t^2. The modulation power efficiency of the 0.1-mm waveguide device was enhanced by a factor of 11 compared with that of 0.5-mm bulk devices.

4. Design and Fabrication of the Waveguide Frequency Shifter

Figure 4 schematically shows the waveguide frequency shifter. Periodic domain inversion was performed on a CLT

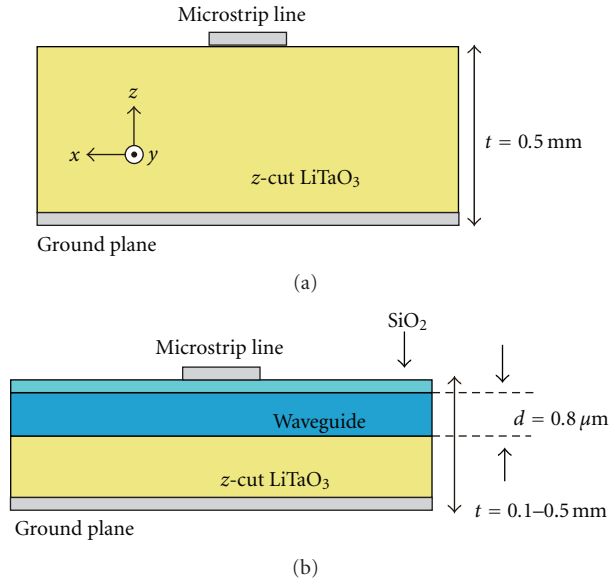

Figure 2: Schematic view of the frequency shifter. (a) Cross-section view of the conventional bulk device. (b) Cross-section view of the waveguide device.

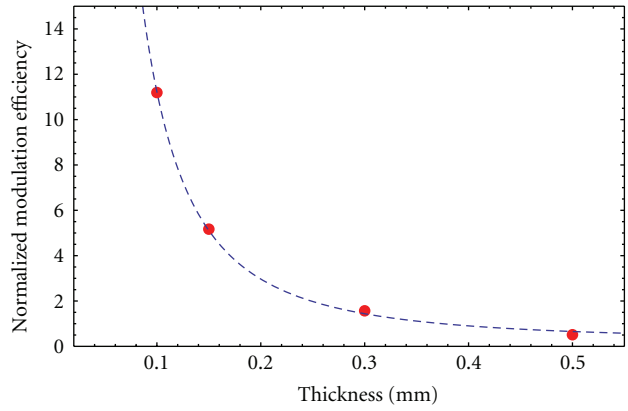

Figure 3: Modulation efficiency normalized by that of the 0.5-mm bulk device. The dashed curve is the theoretical curve fitted to the data.

substrate with the period of $\Lambda_p = 60\,\mu$m. The interaction length was 34 mm. The thickness of the substrate was 0.1 mm. An extraordinary refractive index n_s and a group refractive index n_g of the CLT substrate were calculated to be $n_s = 2.21$ and $n_g = 2.41$, respectively, using the Sellmeier equation for 514.5 nm (Ar laser) [13]. The refractive index of the waveguide was measured to be $n_f = 2.26$. The refractive index of the SiO_2 buffer layer was also calculated to be 1.47, using the Sellmeier equation [14]. Using these refractive indices, the depth of the optical waveguide was designed to be $d = 0.8\,\mu$m, based on mode calculation using effective index method to realize a single TM-guided mode operation.

The 0.8-μm waveguide was fabricated based on the standard proton exchange technique using melted benzoic acid. The temperature of the melted benzoic acid for

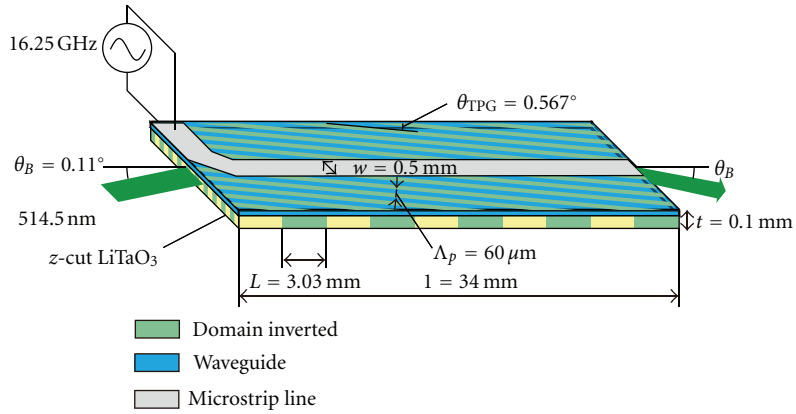

Figure 4: Schematic view of the waveguide frequency shifter.

the proton exchange was set at 240 degrees Celsius. The relation between the exchanging time (t_{ex}) and the depth (d) of the waveguide can be expressed as $d = 2\sqrt{D_{ex}t_{ex}}$, where $D_{ex} = 8.41 \times 10^{-2}(\mu m^2/h)$ [15]. The exchanging time was set to 2 hours. After the exchanging, the device was thermally annealed for 30 minutes at 400 degrees Celsius to reduce the propagation losses and recover the Pockels effect.

The effective relative permittivity for the modulation microwave should be calculated to determine the half period L of the domain inversion. We calculated the effective relative permittivity using an electromagnetic field simulator (method of moments). Figure 5 shows the results. The filled circles represent results of the simulations without SiO_2 buffer layer. The solid line is calculated using the accurately approximate formula for isotropic substrate [16]. The formula is well fitted to the simulated results, therefore the effective relative permittivity with the SiO_2 buffer layer can be calculated through the simulation (open circles in Figure 3). From the simulated result, the phase velocity of the modulation microwave for $t = 0.1$ mm substrate can be determined to be $v_m = 5.48 \times 10^7$ m/s. Together with the group velocity of the optical wave, the half period of the domain inversion for $t = 0.1\,\mu$m is determined as $L = 3.03$ mm using (1).

The tilting angle of the domain inversion was $\theta_{TPG} = \arcsin(\Lambda_p/(2L)) = 0.567°$. The Bragg angle was $\theta_B = \arcsin(\lambda/(2\Lambda)) = 0.11°$, where λ is the wavelength of the optical wave in the crystal and $\Lambda = \Lambda_p/\sqrt{1 - (\Lambda_p/(2L))^2}$.

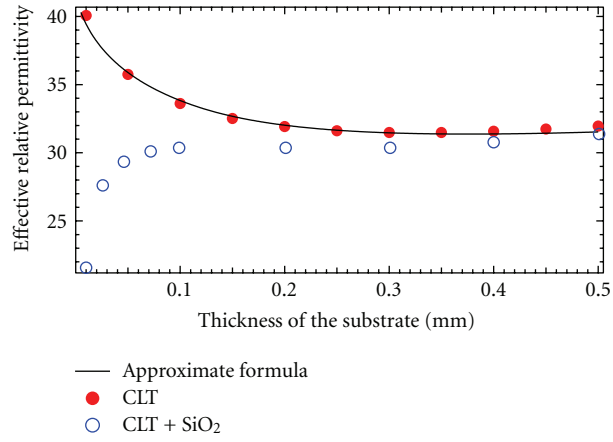

Figure 5: Effective relative permittivity of the microstrip line. Filled and open circles are calculated based on the electromagnetic field simulator (method of moments) for the substrate of CLT only and CLT with SiO_2 buffer layer, respectively. The solid curve is calculated using an accurately approximate formula for the isotropic substrate.

5. Experimental Results and Discussion

The frequency of the modulation signal was 16.25 GHz, which was supplied from a signal generator and amplified by a commercially available power amplifier (R&K: AA380). The available maximum modulation power was 3 W.

Figure 6 shows the frequency-resolved far-field pattern of the output beam. The frequency of the output beam is resolved to the vertical direction with the diffraction grating and the Fourier transform mirror, therefore the horizontal axis is space, whereas the vertical axis corresponds to the frequency. The modulation power was about 1.7 W. We observed two optical beam spots resolved in both space and frequency. The frequency of the 1st diffracted component was shifted by 16.25 GHz and there were no unwanted components at this modulation power. We define the frequency shifting efficiency as the output power ratio of the 1st order diffracted components to the whole output optical power. A frequency shifting efficiency of about 50% was achieved at the modulation power of 1.7 W.

Figure 7 shows the diffraction efficiency of the 1st order of the diffracted component as a function of the square root of the modulation power. The dashed curve is the theoretical curve fitted to the data. A diffraction efficiency of about 65% was achieved at the modulation power of 3 W. About 35% of the optical power was observed in other diffracted components, such as 1st and 2nd order diffracted components. From the fitting, we conclude that the maximum diffraction efficiency can be achieved at the modulation power of 3.6 W.

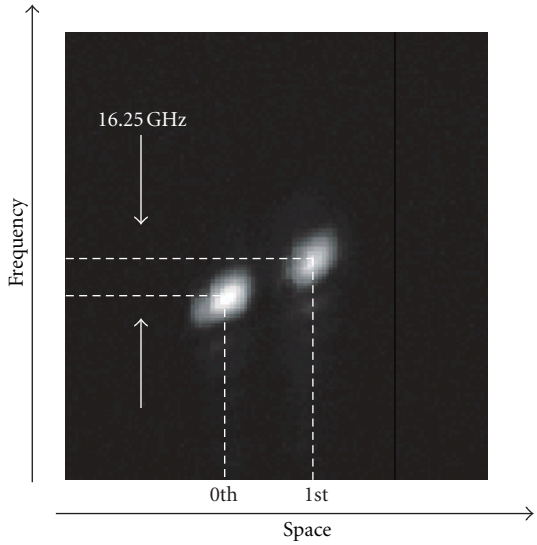

Figure 6: Far-field pattern of the output beam with resolved frequency. The horizontal axis is space. The vertical axis corresponds to the frequency.

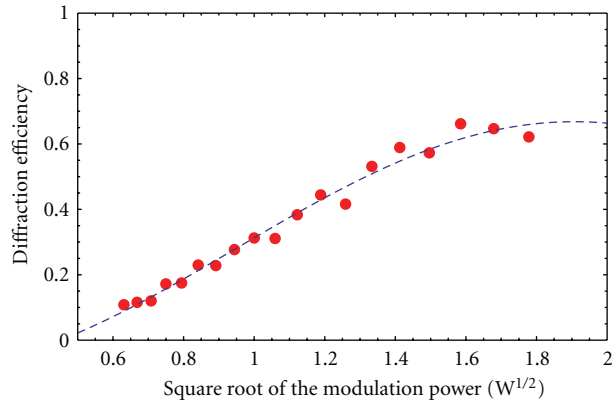

Figure 7: Diffraction efficiency as a function of the square root of the modulate power. The filled circles show the experimental data. The dashed curve shows the theoretical curve fitted to the data.

Previously, we achieved the maximum diffraction efficiency at the modulation power of about 300 W for the interaction length of 12.5 mm in the 0.5-mm bulk device [9]. Compensating the difference of the interaction length, the power efficiency of the current waveguide device should be improved by a factor of 84, which corresponds to the expected modulation power of 3.8 W. The achieved value of 3.6 W is close to this predicted value.

On the other hand, the maximum diffraction efficiency we achieved with the 0.5-mm bulk device was 82% [8]. The degradation of the diffraction efficiency might be due to the degradation of the Q factor of the device. The boundary between the Bragg regime and Raman-Nath regime can be described in terms of the so-called Q factor, given by $Q = 2\pi\lambda l/\Lambda^2$. The Q factor of the current waveguide device was 13.5, whereas that of the former bulk device was 23. Shortening the period of the domain inversion will recover the diffraction efficiency.

We confirmed experimentally the improvement of the modulation power efficiency at 514.4 nm by reducing the gap distance between the hot and ground electrode of the microstrip line. Operation of the shifter at 1550 nm requires further improvement of the modulation power efficiency, by factor of 9. It can be achieved by narrowing the gap to about 0.03 mm for a 34-mm-long device. The 0.03-mm-thick device can be fabricated by the mechanical polishing with the proton exchange process. Crystal ion slicing and wafer bonding (smart guide) [17] is another technique to fabricate the thin-film device without degradation of the optical quality compared with the bulk crystal. Rabiei and Steier demonstrated a $LiNbO_3$ waveguide modulator at 1550 nm with a low propagation loss in which the waveguide was fabricated using the smart guide [18]. Using Sellmeier equation, the group refractive index is calculated to be about 2.17 for 1550 nm, which requires slight modification of the period of the domain inversion for the QVM condition. On the other hand, the propagation characteristics of a thin-film microstrip line can be calculated using equivalent-circuit model [19]. The effective relative permittivity for the 0.03-mm-thick microstrip line with the SiO_2 buffer layers is estimated to be about 28. Using calculated values of the group refractive index for 1550 nm and the effective relative permittivity, the modified half-period of the periodic domain inversion is calculated to be 2.96 mm. The Q factor of the device with 60 μm domain inversion at 1550 nm will be about 40, which promises the frequency conversion efficiency of more than 80% [8]. It is feasible to implement the frequency shifter for the 1550 nm band operating at 16 GHz with more than 80% efficiency.

Improvement of the modulation power efficiency will increase the operation frequency of the device. The thin-film microstrip line supports the THz wave transmission, although stronger attenuation appears above 300 GHz, which is caused by an increasing amount of radiation loss [20]. A 2 W Q-band (30 to 50 GHz) power amplifier is commercially available. Our technique would promise to fabricate the low-loss upconverter which connects the millimeter-wave and 1550 nm optical wave.

6. Conclusion

We proposed waveguide-based frequency shifter, in which modulation power efficiency is improved by a factor of 11 compared with the conventional bulk device. At the modulation power of 3 W, we achieved a frequency shifting of 16.25 GHz with the efficiency of 65%. Improvement of the modulation power efficiency enabled us to demonstrate the continuous operation of the shifting.

Acknowledgment

This research was partially supported by a Grant from the Grant-in-Aid for Challenging Exploratory Research (23656049) from the Ministry of Education, Culture, Sports, Science, and Technology of Japan and a Grant Program

from the Feasibility Study Stage in Adaptable and Seamless Technology Transfer Program (FS-stage, A-STEP).

References

[1] Ze Li, X. Zhang, H. Chi, S. Zheng, X. Jin, and J. Yao, "A reconfigurable microwave photonic channelized receiver based on dense wavelength division multiplexing using an optical comb," *Optics Communications*, vol. 285, pp. 2311–2315, 2012.

[2] D. J. Lee and J. F. Whitaker, "Bandwidth enhancement of electro-optic sensing using high-even-order harmonic sidebands," *Optics Express*, vol. 17, no. 17, pp. 14909–14917, 2009.

[3] M. Tsuchiya, K. Sasagawa, A. Kanno, and T. Shiozawa, "Live electrooptic imaging of W-band waves," *IEEE Transactions on Microwave Theory and Techniques*, vol. 58, no. 11, pp. 3011–3021, 2010.

[4] H. J. Song, N. Shimizu, T. Furuta, K. Suizu, H. Ito, and T. Nagatsuma, "Broadband-frequency-tunable sub-terahertz wave generation using an optical comb, AWGs, optical switches, and a uni-traveling carrier photodiode for spectroscopic applications," *Journal of Lightwave Technology*, vol. 26, no. 15, pp. 2521–2530, 2008.

[5] A. Hirata, T. Kosugi, H. Takahashi et al., "120-GHz-band millimeter-wave photonic wireless link for 10-Gb/s data transmission," *IEEE Transactions on Microwave Theory and Techniques*, vol. 54, no. 5, pp. 1937–1942, 2006.

[6] T. K. Woodward, A. Agarwal, T. Banwell et al., "Systems perspectives on optically-assisted RF signal processing using silicon photonics," in *Proceedings of the IEEE International Topical Meeting on Microwave Photonics*, pp. 377–380, October 2011.

[7] A. Agarwal, T. Banwell, and T. K. Woodward, "Optically filtered microwave photonic links for RF signal processing applications," *Journal of Lightwave Technology*, vol. 29, no. 16, Article ID 5957251, pp. 2394–2401, 2011.

[8] K. Shibuya, S. Hisatake, and T. Kobayashi, "10-GHz-order high-efficiency electrooptic frequency shifter using slant-periodic domain inversion," *IEEE Photonics Technology Letters*, vol. 16, no. 8, pp. 1939–1941, 2004.

[9] S. Hisatake, T. Konishi, and T. Nagatsuma, "Multiplication of optical frequency shift by cascaded electro-optic traveling phase gratings operating above 10 GHz," *Optics Letters*, vol. 36, no. 8, pp. 1350–1352, 2011.

[10] M. Chaciski and U. Westergren, "100 GHz electro-optical modulator chip," in *Proceedings of the Optoelectronics and Communications Conference (OECC '11)*, pp. 59–60, 2011.

[11] K. Tada, T. Murai, T. Nakabayashi, T. Iwashima, and T. Ishikawa, "Fabrication of $LiTaO_3$ optical waveguide by H+ exchange method," *Japanese Journal of Applied Physics, Part 1*, vol. 26, no. 3, pp. 503–504, 1987.

[12] I. Savatinova, S. Tonchev, R. Todorov, M. N. Armenise, V. M. N. Passaro, and C. C. Ziling, "Electro-optic effect in proton exchanged $LiNbO_3$ and $LiTaO_3$ waveguides," *Journal of Lightwave Technology*, vol. 14, no. 3, pp. 403–409, 1996.

[13] K. S. Abedin and H. Ito, "Temperature-dependent dispersion relation of ferroelectric lithium tantalate," *Journal of Applied Physics*, vol. 80, no. 11, pp. 6561–6563, 1996.

[14] C. M. Herzinger, B. Johs, W. A. McGahan, J. A. Woollam, and W. Paulson, "Ellipsometric determination of optical constants for silicon and thermally grown silicon dioxide via a multi-sample, multi-wavelength, multi-angle investigation," *Journal of Applied Physics*, vol. 83, no. 6, pp. 3323–3336, 1998.

[15] P. J. Matthews, A. R. Mickelson, and S. W. Novak, "Properties of proton exchange waveguides in lithium tantalate," *Journal of Applied Physics*, vol. 72, no. 7, pp. 2562–2574, 1992.

[16] M. Kobayashi and R. Terakado, "Accurately approximate formula of effective filling fraction for microstrip line with isotropic substrate and its application to the case with anisotropic substrate," *IEEE Transactions on Microwave Theory and Techniques*, vol. 27, no. 9, pp. 776–778, 1979.

[17] P. Rabiei and P. Gunter, "Optical and electro-optical properties of submicrometer lithium niobate slab waveguides prepared by crystal ion slicing and wafer bonding," *Applied Physics Letters*, vol. 85, no. 20, pp. 4603–4605, 2004.

[18] P. Rabiei and W. H. Steier, "Lithium niobate ridge waveguides and modulators fabricated using smart guide," *Applied Physics Letters*, vol. 86, no. 16, Article ID 161115, pp. 1–3, 2005.

[19] F. Schnieder and W. Heinrich, "Model of thin-film microstrip line for circuit design," *IEEE Transactions on Microwave Theory and Techniques*, vol. 49, no. 1, pp. 104–110, 2001.

[20] M. Nagel, T. Dekorsy, M. Brucherseifer, P. Haring, and B. H. Kurz, "Characterization of polypropylene thin-film microstrip lines at millimeter and submillimeter wavelengths," *Microwave and Optical Technology Letters*, vol. 29, no. 2, pp. 97–100, 2001.